ARTICLE IN PRESS

Communications Engineering

https://doi.org/10.1038/s44172-026-00626-3

Article in Press

3D reconstruction and etching profile simulation for wiggling active area effect in dynamic random access memory manufacturing

Received: 12 September 2025

Accepted: 17 February 2026

Ziyi Hu, Jing Wen, Chaoran Yang, Hua Shao, Yuxuan Zhai, Rui Ge, Xiaobin He, Zongzheng Men, Yi Yang, Dianming Sun, Zhongming Liu, Dashan Shang, Zhiqiang Li, Junjie Li, Lado Filipovic, Rui Chen & Ling Li

Cite this article as: Hu, Z., Wen, J., Yang, C. *et al.* 3D reconstruction and etching profile simulation for wiggling active area effect in dynamic random access memory manufacturing. *Commun Eng* (2026). https://doi.org/10.1038/s44172-026-00626-3

We are providing an unedited version of this manuscript to give early access to its findings. Before final publication, the manuscript will undergo further editing. Please note there may be errors present which affect the content, and all legal disclaimers apply.

If this paper is publishing under a Transparent Peer Review model then Peer Review reports will publish with the final article.

ARTICLE IN PRESS

© The Author(s) 2026. **Open Access** This article is licensed under a Creative Commons Attribution-NonCommercial-NoDerivatives 4.0 International License, which permits any non-commercial use, sharing, distribution and reproduction in any medium or format, as long as you give appropriate credit to the original author(s) and the source, provide a link to the Creative Commons licence, and indicate if you modified the licensed material. You do not have permission under this licence to share adapted material derived from this article or parts of it. The images or other third party material in this article are included in the article's Creative Commons licence, unless indicated otherwise in a credit line to the material. If material is not included in the article's Creative Commons licence and your intended use is not permitted by statutory regulation or exceeds the permitted use, you will need to obtain permission directly from the copyright holder. To view a copy of this licence, visit http://creativecommons.org/licenses/by-nc-nd/4.0/.

ARTICLE IN PRESS

3D Reconstruction and Etching Profile Simulation for Wiggling Active Area Effect in Dynamic Random Access Memory Manufacturing

Ziyi Hu[1,2], Jing Wen[1], Chaoran Yang[1,2,3], Hua Shao[1], Yuxuan Zhai[1,2], Rui Ge[1], Xiaobin He[1], Zongzheng Men[3], Yi Yang[3], Dianming Sun[3], Zhongming Liu[3], Dashan Shang[1,2], Zhiqiang Li[1], Junjie Li[1*], Lado Filipovic[4*], Rui Chen[1*], Ling Li[1,2]

[1]State Key Laboratory of Fabrication Technologies for Integrated Circuits, Institute of Microelectronics, Chinese Academy of Sciences, Beijing 100029, China

[2]School of Integrated Circuits, University of Chinese Academy of Sciences, Beijing 100049, China

[3]Changxin Memory Technologies Inc., Hefei 230031, Anhui, China

[4]CDL for Multi-Scale Process Modeling of Semiconductor Devices and Sensors, Institute for Microelectronics, TU Wien, 1040 Viena, Austria

[*]Corresponding authors: lijunjie@ime.ac.cn; chenrui1@ime.ac.cn; filipovic@iue.tuwien.ac.at

ARTICLE IN PRESS

ARTICLE IN PRESS

Abstract

Dynamic Random Access Memory (DRAM), a critical component in modern computing systems, relies heavily on the structural integrity of its active area (AA) - a fin-shaped transistor region responsible for charge transfer in memory cells. During advanced DRAM fabrication, the plasma etching process often induces shape distortions in the AA region (termed "wiggling AA"), which degrade capacitive charging/discharging efficiency and device reliability. While this phenomenon is widely observed in industry, its mechanistic origins remain poorly understood, necessitating systematic investigation to enable precision etching control. In this paper, we fabricated active area transistors of DRAM structures and characterized the etching results using three-dimensional (3D) reconstruction based on focused ion beam-scanning electron microscopy (FIB-SEM) data. In parallel, we developed a 3D etching feature profile model that correlates process parameters with structural deformation and simulated the etching process under three oxygen flow rates. By integrating experimental data and simulation results, we systematically analyzed the mechanistic origins of the wiggling AA effect and demonstrated improvement by modulating the oxygen flow rate. This study bridges the gap between empirical observations and fundamental etching mechanisms, offering actionable strategies for optimizing high-density DRAM manufacturing processes.

Keywords

DRAM, Wiggling AA, Etching, 3D Reconstruction, Process Simulation

ARTICLE IN PRESS

Introduction

Dynamic Random Access Memory (DRAM), a cornerstone of modern computing and electronic systems, dominates the global memory chip market due to its high-speed data storage capabilities [1-3]. In mainstream DRAM architectures, the 1T1C (one-transistor-one-capacitor) memory cell remains the industry standard, where the capacitor stores charge and the transistor regulate charge transfer through the capacitor [4]. A critical element in DRAM arrays is the active area (AA) - a fin-like transistor structure that governs device performance and scalability [5]. In an advanced $6F^2$ DRAM design, the AA is typically patterned using a hybrid approach combining self-aligned quadruple patterning (SAQP) and Litho-Etch-Litho-Etch (LELE) processes, which enable high-density feature fabrication via a hard mask template (**Figure 1**) [6]. While SAQP and LELE enhance AA density, they introduce significant challenges in subsequent fin etching processes. Notably, shape distortions (termed "wiggling AA") frequently occur during plasma

ARTICLE IN PRESS

etching, manifesting as non-uniform sidewall profiles or fin curvature [7-8]. These distortions degrade charge retention in capacitors and disrupt transistor switching dynamics, ultimately compromising device reliability. Therefore, achieving high-precision control of the etching process is critical to suppressing wiggling AA defects and ensuring DRAM performance at scaled technology nodes.

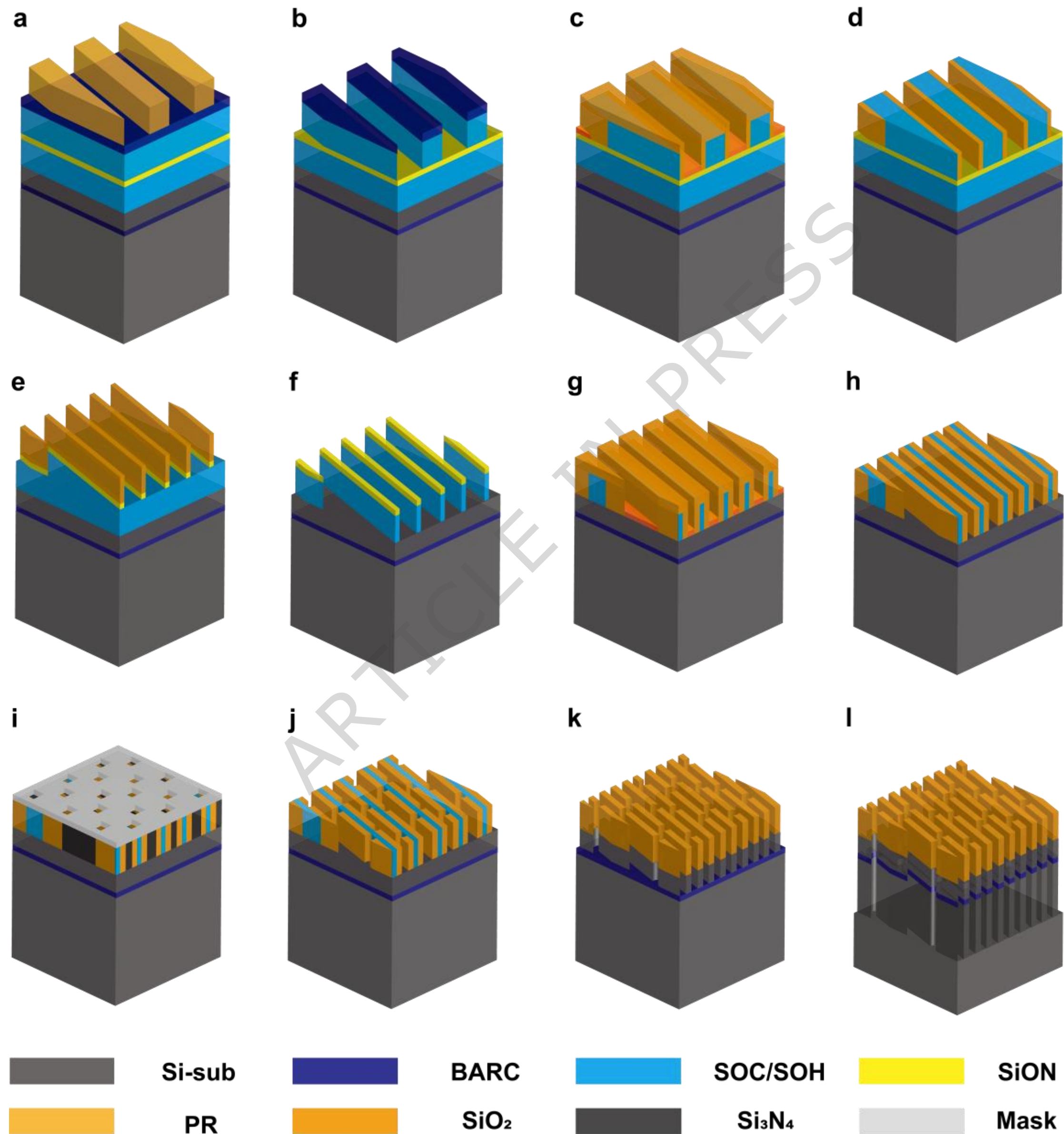

Figure 1. Schematic diagram illustrating the industrial etching process flow for creating the DRAM active area, typically involving SAQP and LELE techniques. (Note that the specific experimental structures in this study were fabricated using Electron Beam Lithography (EBL) to replicate key features of these dense patterns.). All transitions in the schematic are shown with

ARTICLE IN PRESS

uniform feature sizes for simplicity. a) Resist exposure-1, b) Core etch-1, c) Atomic layer deposition-1, d) Spacer etch-1, e) Strip core-1, f) Core etch-2, g) Atomic layer deposition-2, h) Spacer etch-2, i) Resist exposure-2, j) Hole etch, k) Strip core-2, l) Substrate etch.

An accurate characterization of the results is a prerequisite for precise control of the etching process. The characterization of general etching processes typically relies on traditional methods such as scanning electron microscopy (SEM) and transmission electron microscopy (TEM), which only provide two-dimensional (2D) top-down views or limited cross-sectional information [9]. This is insufficient for analyzing the etched profile of complex AA regions in DRAM structures. In contrast, three-dimensional (3D) reconstruction can deliver comprehensive 3D structural data, enabling engineers to more accurately evaluate etching outcomes, including enhanced precision in process control, detection of intricate 3D structural defects, optimization of process parameters, and significant reduction in trial-and-error costs. Common 3D reconstruction techniques include focused ion beam-scanning electron microscopy (FIB-SEM) and X-ray computed tomography (X-ray CT), which have been widely applied in fields such as materials science, biomedical research, and manufacturing [10-13]. For the nanoscale etch profile characterization required in this study, the ~1 nm resolution of FIB-SEM is indispensable, whereas the micron-scale resolution of non-destructive X-ray CT proves inadequate (see **Table 1**) [14]. The FIB-SEM technique, which combines ion beam milling with electron beam imaging, operates through alternating cycles of material removal and imaging, enabling layer-by-section 3D reconstruction [15]. This method allows for complex 3D morphology analysis and defect localization in semiconductor materials, despite its current practical resolution being limited to the 5-50 nm range due to challenges such as ion beam-induced sample damage and serial section alignment accuracy [16].

ARTICLE IN PRESS

Table 1: Comparison between FIB-SEM and MicroCT for Microelectronics Applications

Parameter	FIB-SEM	MicroCT[14]	Requirements for This Study
Spatial Resolution	~1-5 nm (Ultra-high)	~0.5-5 µm (Limited)	Nanometer-scale precision
Volume Size	~1×1×1 µm³ (Local)	~1×1×1 cm³ (Bulk)	Specific device arrays
Acquisition Time	Slow (Hours to days)	Fast (Minutes to hours)	Time well invested
Sample Prep.	Complex (requires specific size)	Simple (often non-destructive)	Necessary trade-off
Destructive	Yes	No	Post-analysis disposal

ARTICLE IN PRESS

Primary Applications	Nanoscale device structure, failure analysis, circuit edit	Package-level defects, 3D packaging, TSV	Nanoscale etch profile

Technology computer aided design (TCAD) is another widely used approach for investigating and optimizing etching process mechanisms [17]. There have been relevant studies which investigate the reaction mechanism of the etching process by establishing 3D physics-based models [17-21]. Research on finite-length structures has examined profiles under both angularly asymmetric and symmetric ion flux conditions. This work found that profiles generated by 3D simulators exhibit greater sidewall sloping at three-plane corners than those predicted by 2D simulations [17]. Subsequent development and application of a 3D profile simulator, the Monte Carlo feature profile model, has enabled the investigation of etching dependencies on aspect ratio and feature orientation [18]. Therefore, to address the complex mechanisms and geometric effects during advanced DRAM etching, integrating 3D reconstruction with 3D process simulation enables the acquisition of 3D experimental data to calibrate 3D models. These calibrated models are then able to predict outcomes under varying parameters during process optimization, thereby significantly reducing the number of experimental iterations. Furthermore, the synergy between experimental and computational approaches facilitates a deeper understanding of etching mechanisms - such as ion flux distribution, chemical reaction kinetics, and material selectivity - ultimately supporting process optimization for high-aspect-ratio structures and defect minimization.

ARTICLE IN PRESS

In this study, to investigate the wiggling AA effect observed during plasma etching in advanced DRAM architectures, we fabricated the active area transistors under laboratory conditions using EBL and inductively coupled plasma (ICP) dry etching to replicate key features of the dense DRAM structures. The etching results were characterized through SEM and 3D reconstruction based on FIB-SEM data. In parallel, we developed a 3D etching feature profile model that correlates process parameters with structural deformation and systematically simulated the etching process under three oxygen flow rates (2, 3, and 4.5 sccm). By combining experimental data and simulation results, we systematically analyzed the mechanistic origins of the wiggling AA effect and quantified the role of oxygen flow rate in modulating this phenomenon. Section II presents the 3D reconstruction of experimental results, 3D model simulation outcomes, and a quantitative analysis of the oxygen flow rate on the modulation of the wiggling AA effect. Section III details the fabrication and reconstruction workflows of the AA structure and the framework of the proposed 3D etching model. Section IV summarizes the key conclusions and implications for process optimization.

ARTICLE IN PRESS

Results and discussions

Wiggling AA experimental characterization based on 3D reconstruction

To investigate the wiggling AA effect of the etching profile in the DRAM, we first designed a fin array structure of DRAM and carried out etching experiments. The pattern design of the fin array is shown in **Figure 2(f)** and consists of staggered rectangles. To obtain different degrees of the wiggling AA effect, we kept other conditions unchanged and set up three experiments with different oxygen flow rates, which were 2 sccm, 3 sccm and 4.5 sccm respectively. We use SEM to characterize the etching results, as shown in **Figure 2(a-c)**. **Figure 2(d)** shows the wiggling AA phenomena, which occurs frequently in the etching profile of active areas during DRAM manufacturing by mainstream manufacturers [8]. In our study, the etching process consisted of two steps: an initial oxide etch followed by a silicon etch. In the top-view image of the active area obtained after the silicon etch (**Figure 2(e)**), we observed similar wiggling phenomena. This indicates that the etching mechanism in our experiments is closer to that of mainstream manufacturers' DRAM active areas, and analyzing these experimental results can provide better understanding of the underlying physical mechanisms. However, traditional methods such as SEM and TEM only provide 2D top-down views or limited cross-sectional information. This is insufficient for analyzing the etching of complex AA regions in DRAM structures. Therefore, to characterize the etching profile of active areas, we employed a FIB-SEM-based 3D reconstruction methodology on the result with an oxygen flow rate set to 2 sccm. Initially, FIB tomography was utilized to acquire a dataset of 300 SEM images, as illustrated in **Figure 2(g)**. The image stack was subsequently aligned and processed using the Dragonfly software [22], where deep learning-based segmentation algorithms, combined with volumetric rendering techniques were implemented to perform 3D reconstruction. **Figure 2(h)** shows the reconstructed 3D morphology, demonstrating the effectiveness of this analytical approach.

ARTICLE IN PRESS

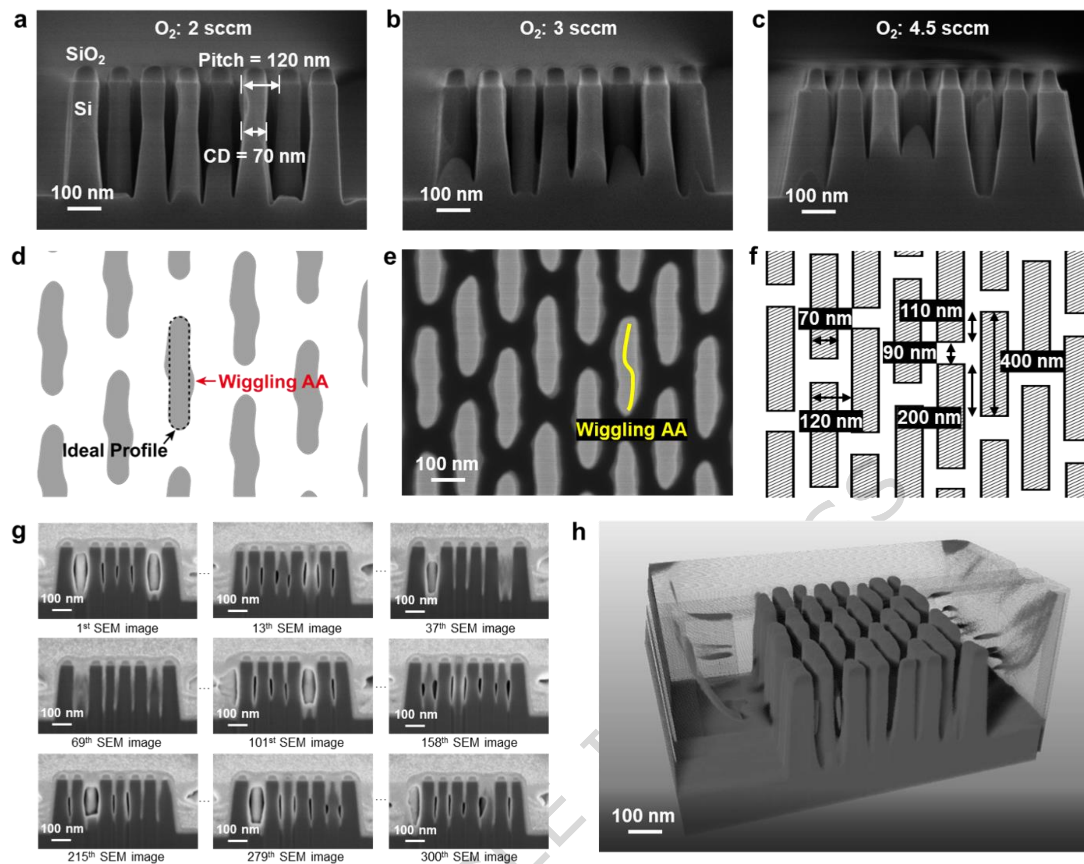

Figure 2. Characterization of AA etching results and the wiggling AA effect in DRAM active array manufacturing. a-c) SEM characterization of AA etching results at different oxygen flow rates, d) Wiggling AA effect during DRAM manufacturing, e) Wiggling AA effect appears in the top view of the topography after etching when we manufactured the DRAM active array, f) The mask pattern we designed when manufacturing DRAM active arrays, g) Several samples from the 300 SEM images obtained by FIB-SEM method for 3D reconstruction dataset, h) 3D reconstruction result (For dynamic display, please refer to Supplementary Video 1).

Following the 3D reconstruction, comprehensive morphological characterization was achieved through a multi-perspective analysis. As shown in **Figure 3(a, b)**, the external surface profile could be examined from multiple angles. Leveraging the advanced functionalities of the Dragonfly software, cross-sectional slicing along different 2D planes was performed to probe internal structural features. Three cross-sectional planes at progressively deeper positions (Z1 < Z2 < Z3) were analyzed (**Figure 3(c-e)**), revealing that the wiggling AA effect became increasingly pronounced with depth, accompanied by a systematic expansion of fin widths. This trend, also observable in conventional SEM cross-sections (**Figure 2(a-c)**), is attributed to the higher etching

ARTICLE IN PRESS

rate at the top region compared to the bottom.

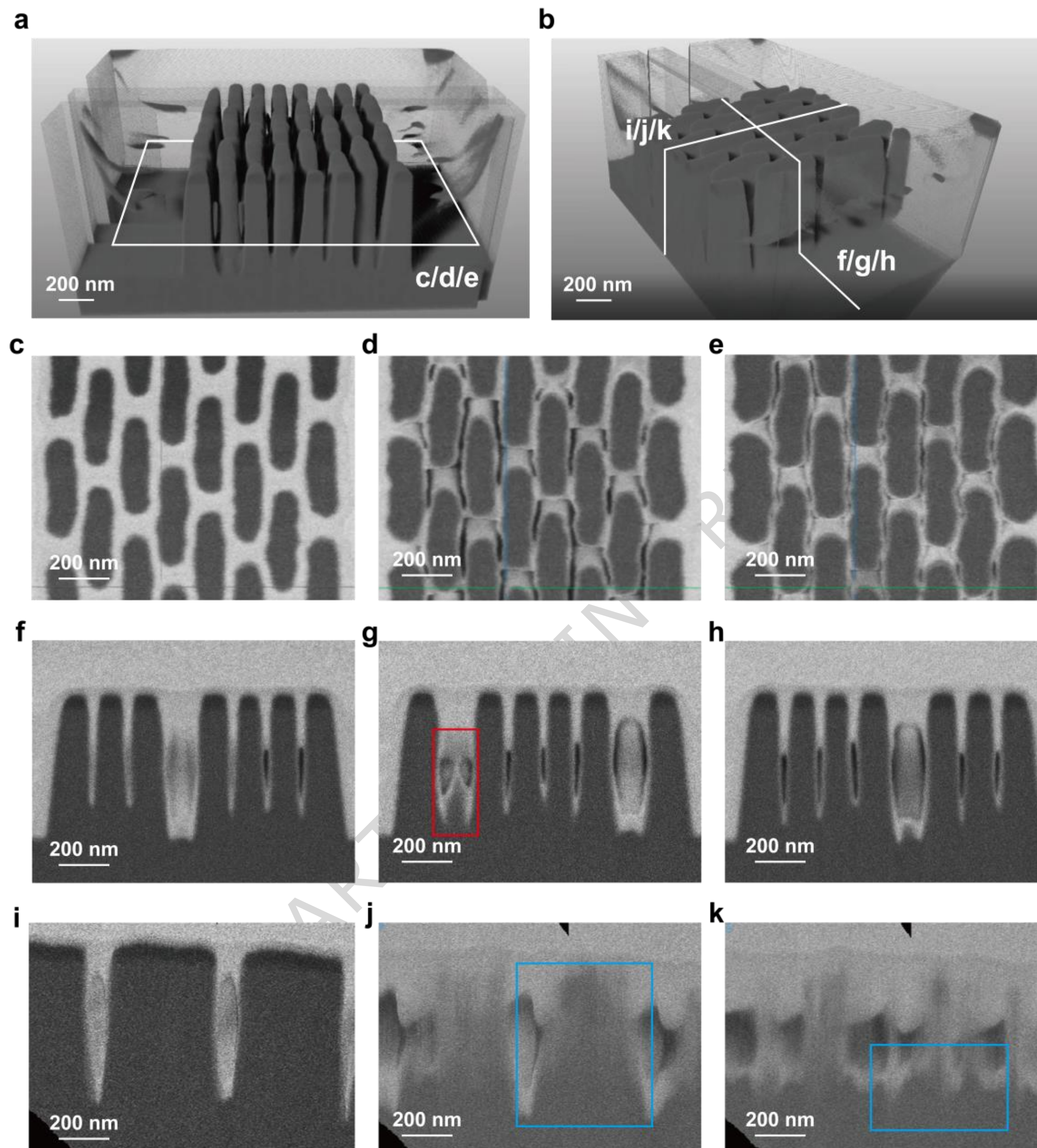

Figure 3. 3D reconstruction of the DRAM active area and corresponding cross-sectional views. a-b) Two perspectives of the reconstructed structure, with labeled planes indicating the slicing directions used for the subsequent subfigures. c-e) Cross-sections taken parallel to the wafer surface at progressively deeper positions along the c/d/e axis, the green lines mark the observation positions corresponding to the transition from (f) to (h), while the faint blue lines mark the positions corresponding to the series from (i) to (k). f-h) Cross-sections taken parallel to the SEM imaging plane at different positions along the f/g/h axis, the red box in (g) highlights a region

ARTICLE IN PRESS

exhibiting a "bamboo shoot emerging from soil" morphology. i-k) Cross-sections taken perpendicular to the SEM imaging plane at different positions along the i/j/k axis, the blue boxes in (j) and (k) delineate the interstitial region between parallel fins.

For comparative validation, morphological features matching the SEM cross-sectional viewing angles were reconstructed (**Figure 3(f-h)**). Unlike conventional SEM techniques that suffer from positional uncertainty due to structural complexity and stochastic sampling, our 3D reconstruction enabled continuous tracking of fin morphology variations. The analysis demonstrated significant spatial heterogeneity in fin integrity, exhibiting alternating patterns of complete structures and localized material loss. Furthermore, orthogonal cross-sections relative to SEM imaging planes were reconstructed (**Figure 3(i)**), revealing fully resolved structures that would be inaccessible through conventional SEM or TEM approaches due to positioning challenges. In contrast, the indistinct features observed in **Figure 3(j, k)** correspond to the interstitial region between parallel fins, where only the unetched bottom portion remained visible, providing critical insights into basal etching roughness. This 3D reconstruction methodology provides high spatial resolution and analytical flexibility for investigating complex 3D nanostructures, enabling systematic investigation of etching mechanisms through multi-scale morphological correlations.

ARTICLE IN PRESS

Wiggling AA effect simulation based on 3D etching profile model

While 3D reconstruction provides valuable insights for mechanistic investigations, it also faces practical limitations. These include stage drift caused by mechanical vibrations during prolonged imaging sessions and the significant time required, which restrict extensive characterization across diverse process conditions [23, 24]. To address these constraints, we developed a computational framework integrating Monte Carlo simulations with voxel-based segmentation algorithms for 3D etching profile modeling. As schematically illustrated in **Figure 4(a, b)**, the model architecture fundamentally incorporates Monte Carlo algorithms to simulate reactant flux dynamics and voxel evolution processes during structural etching. The systematic workflow is comprised of four core modules, as demonstrated in **Figure 4(c-e)**: particle flux distribution for quantifying spatial distribution of incident species, Monte Carlo trajectory tracking for modeling particle transport with stochastic collisions, surface reaction dynamics for simulating etching probability functions, and morphological evolution for implementing voxel removal algorithms.

The model was validated through systematic simulations of etching processes under three oxygen flow rates (2, 3, and 4.5 sccm), with mask configurations mirroring experimental designs.

To optimize computational efficiency, a simulation domain of 1500×1000×300 nm³ was implemented with 1 nm voxel^{-1} resolution. **Figure 5(a)** illustrates a 3D visualization of the 2 sccm oxygen flow simulation, where the silicon oxide hard mask is depicted in green and the silicon substrate in cyan. A magnified view in **Figure 5(b)** reveals surface micro-roughness patterns originating from the stochastic nature of particle-surface interactions in Monte Carlo simulations.

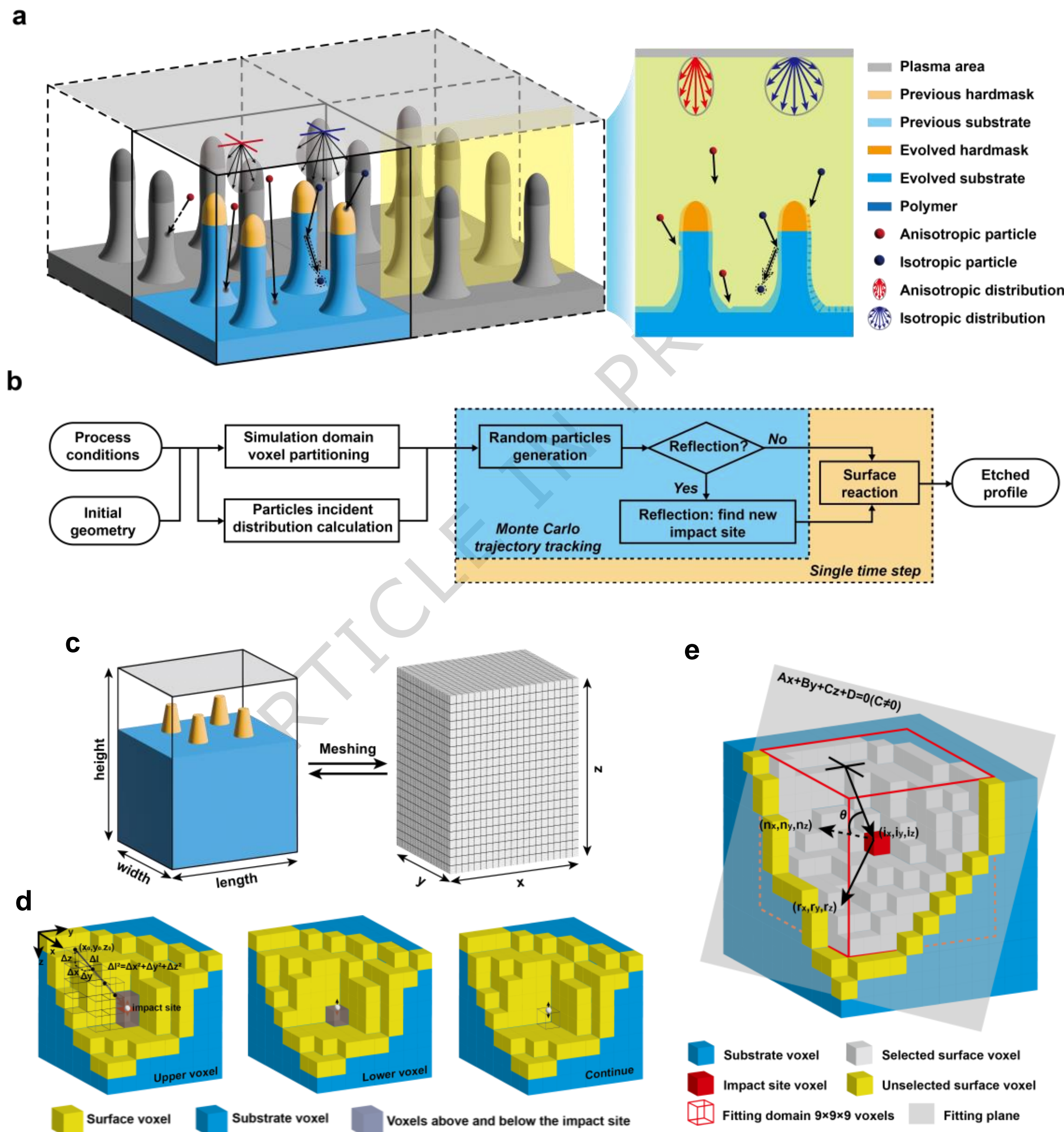

Figure 4. Schematic illustration of the computational model and algorithm principles for three-dimensional simulation. a) Diagram of the simulation domain and particle incident in the three-dimensional model. b) Model algorithm flow diagram. c) Diagram of the three-dimensional simulation domain voxel division, the blue areas correspond to the substrate, and the yellow areas

ARTICLE IN PRESS

correspond to the hardmask. d) Three cases of the Monte Carlo trajectory tracking algorithm in the three-dimensional model. e) The least square method is used to fit the plane and calculate the reflection vector in the three-dimensional model.

Our 3D etching model replicates the cross-sectional analytical capabilities of 3D reconstruction techniques. Benchmarking against the 3D reconstruction method, we first performed 2D cross-sectional analyses on the simulation with the oxygen flow set to 2 sccm at three distinct depths (Z1 = 100 nm, Z2 = 300 nm, Z3 = 500 nm), as shown in **Figure 5(c-e)**. The simulations successfully reproduced the characteristic depth-dependent trends observed experimentally: progressive intensification of wiggling AA and systematic fin width expansion with increasing etch depth. Furthermore, virtual cross-sections matching SEM imaging orientations were likewise reconstructed (**Figure 5(f-h)**), demonstrating spatial heterogeneity in fin morphology that precisely mirrors experimental observations. Notably, the anomalous contour within the red box of **Figure 5(g)** exhibits striking similarity to the "bamboo shoot emerging from soil" morphology observed in the red box of **Figure 3(g)**. This artifact arises when cross-sectional planes intersect fin edge regions, selectively revealing root structures - a phenomenon successfully captured by our model.

ARTICLE IN PRESS

Extended virtual dissection of the simulated structure revealed additional morphological correlations. **Figure 5(i)** displays trench profiles analogous to those in the measured profiles from **Figure 3(i)**, while **Figure 5(j, k)** replicates the interstitial fin spacing characteristics of experiments in **Figure 3(j, k)**. The morphology further demonstrates the model's capability to resolve intermediate structural states. These systematic comparisons confirm that our 3D etching simulation framework achieves comparable analytical performance to 3D reconstruction, while overcoming its intrinsic limitations in complex, time-consuming, and cost-intensive process characterization. This computational approach establishes a robust platform for investigating etching mechanism-property relationships and process parameter optimization.

Study on the mechanism of wiggling AA and the influence of oxygen flow rate

The simulated etching profiles under additional oxygen flow rates (3 sccm and 4.5 sccm) were systematically analyzed through multi-view 2D cross-sectional examinations, as presented in **Figure 6(a-j)**. Comparative analysis of the left and main views revealed a pronounced oxygen flux-dependent tapering effect, where fin sidewalls exhibited progressively more tapered profiles with increasing oxygen flow rate. This trend aligns with the experimental SEM observations shown in **Figure 2(a-c)** across varying oxygen flow rates. While such behavior has previously been reported for simpler geometries such as trenches and cylindrical holes under HBr/O_2 plasmas, our

ARTICLE IN PRESS

work extends this understanding to dense DRAM active-area fin arrays, demonstrating how these mechanisms give rise to the characteristic wiggling AA effect and quantifying its dependence on oxygen flow. Moreover, by combining 3D reconstruction with simulation, our approach enables evaluation of different process conditions and provides guidance on selecting the most appropriate oxygen flow to optimize fin shape and suppress wiggling defects in DRAM fabrication.

ARTICLE IN PRESS

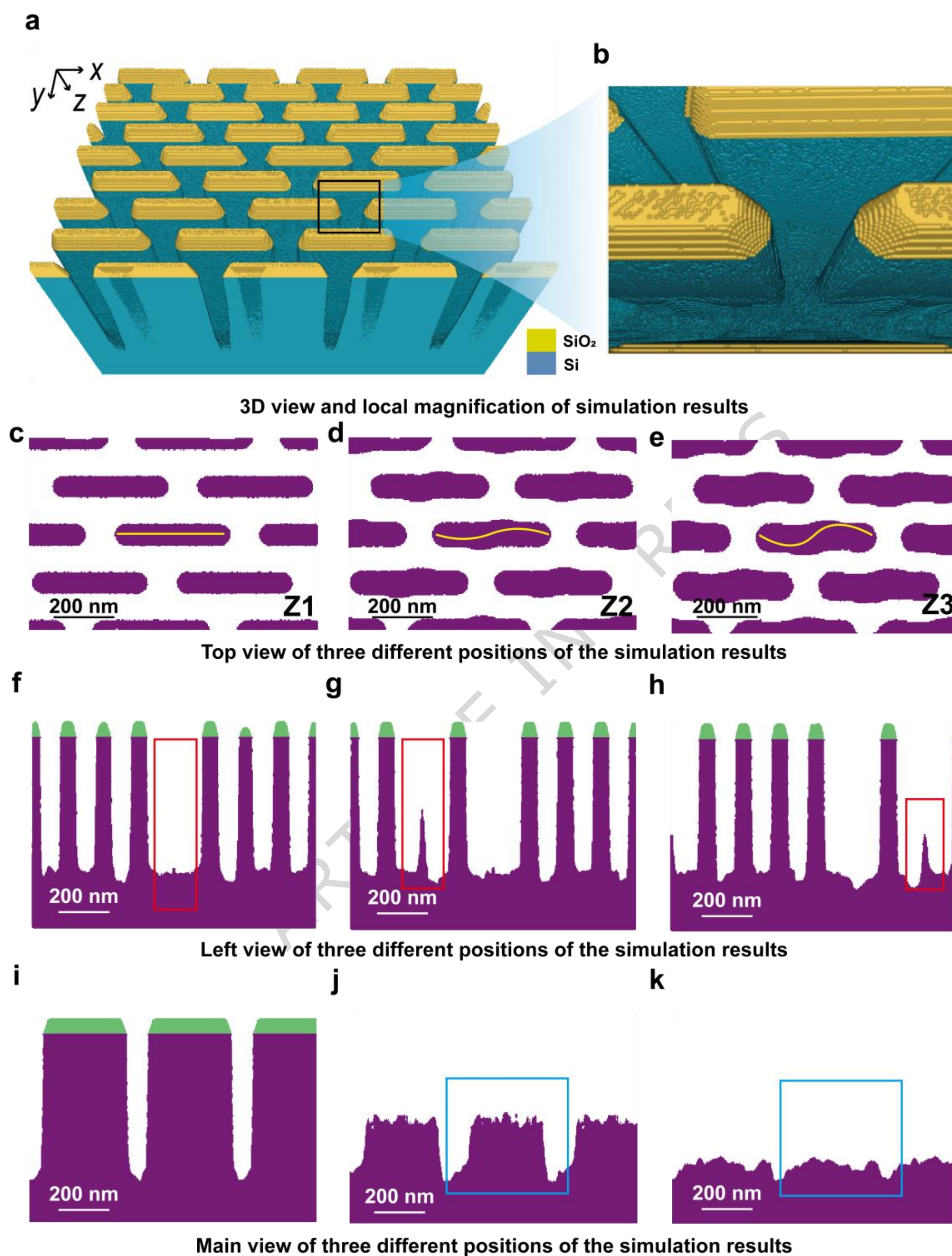

Figure 5. Three-dimensional simulation results and multi-perspective cross-sectional analysis of the etched pillar structure. a) 3D view of the simulation result at an oxygen flow rate of 2 sccm (For dynamic display, please refer to Supplementary Video 2). b) Local magnification of the 3D view result. c-e) show 2D slices of the simulated structure along the depth of the pillars with c

corresponding to the shallowest position (Z1 = 100 nm), d corresponding to the shallowest position (Z2 = 300 nm), and e corresponding to the deepest (Z3 = 500 nm), the yellow lines trace the amplitude of wiggling. f-h) Cross-sections obtained by cutting 2D planes parallel to the SEM shooting surface in the 3D simulation results, the red boxes highlight regions exhibiting the same "bamboo shoot emerging from soil" morphology identified in Figure 3. i-k) Cross-sections obtained by cutting 2D planes perpendicular to SEM shooting surface in the 3D simulation results, the blue boxes mark regions showing the same interstitial features between parallel fins as described in Figure 3. Throughout panels (c-k), the purple and green objects represent the silicon (Si) and silicon dioxide (SiO_2) materials, respectively.

Notably, the simulation unveiled distinct feature-dependent etching behaviors, for example shown in **Figure 6(i)**. Crucially, this occurred even with a well-defined initial mask profile achieved by electron beam lithography, ruling out mask deformation as the primary cause - a factor often emphasized in prior studies attributing similar distortions to mask imperfections [25, 26]. Our observation demonstrates that the wiggling instability can be intrinsically generated during the deep etch process itself. Wide mask openings demonstrated deeper bottom etching compared to narrow openings, accompanied by more tapered sidewall profiles, due to the loading effect [27]. While mechanisms like ion shadowing or mask charging can contribute in some contexts, the strong sensitivity of wiggling severity to the O_2 flow rate - under constant bias power and feature geometry - indicates a mechanism dominated by surface chemical passivation and neutral species transport. This loading effect originates from differential reactant flux distributions - wider openings permit enhanced radical transport to substrate surfaces, simultaneously accelerating vertical etching and promoting sidewall passivation through by-product accumulation. In the HBr/O_2 chemistry used, the volatility of silicon bromide ($SiBr_x$) products [28] is crucial, enabling the efficient transport of etchants and by-products that underpin the observed chemical loading effect. These computational insights provide an in-depth fundamental understanding of plasma-surface interactions, demonstrating our model's capability to resolve complex feature-scale etching heterogeneities that challenge conventional experimental characterization methods.

To quantitatively characterize the degree of the wiggling AA effect, we established a geometric metric based on the ratio of the post-etch fin width (W_{etch}) to the pre-pattern width ($W_{pattern}$), as illustrated in **Figure 6(k)**. This dimensionless parameter, termed the wiggling degree, directly correlates with the magnitude of wiggling AA, higher values indicate more pronounced wiggling phenomena. All the complete fins (five in total) in the top view of **Figure 5(c-e)**, **Figure 6(a-c)**, and **Figure 6(f-h)** are respectively calculated wiggling degrees, and the average results are summarized in **Figure 6(l)**. It should be noted that the three observed depths of the results of

ARTICLE IN PRESS

ARTICLE IN PRESS

different groups are consistent. We found that with increasing the oxygen flow rate, wiggling degrees in different locations all increase to some extent, which is consistent with the wiggling AA formation mechanism previously described: more oxygen leads to more sidewall protection and redeposition. In addition, the wiggling degree of the 2D profile of the 3D reconstruction result is likewise shown in **Figure 6(l)**; this measured result presents the same trend as the simulated results. Therefore, through experiments and simulations, we can conclude that reducing the oxygen flow rate can reduce the wiggling AA effects to a certain extent. At the same time, the reduction of oxygen may also lead to other effects or defects, which are not within the scope of this study and should be subsequently analyzed. Nevertheless, our proposed model can provide actionable insights for the manufacturing process of DRAM and other high aspect ratio devices.

ARTICLE IN PRESS

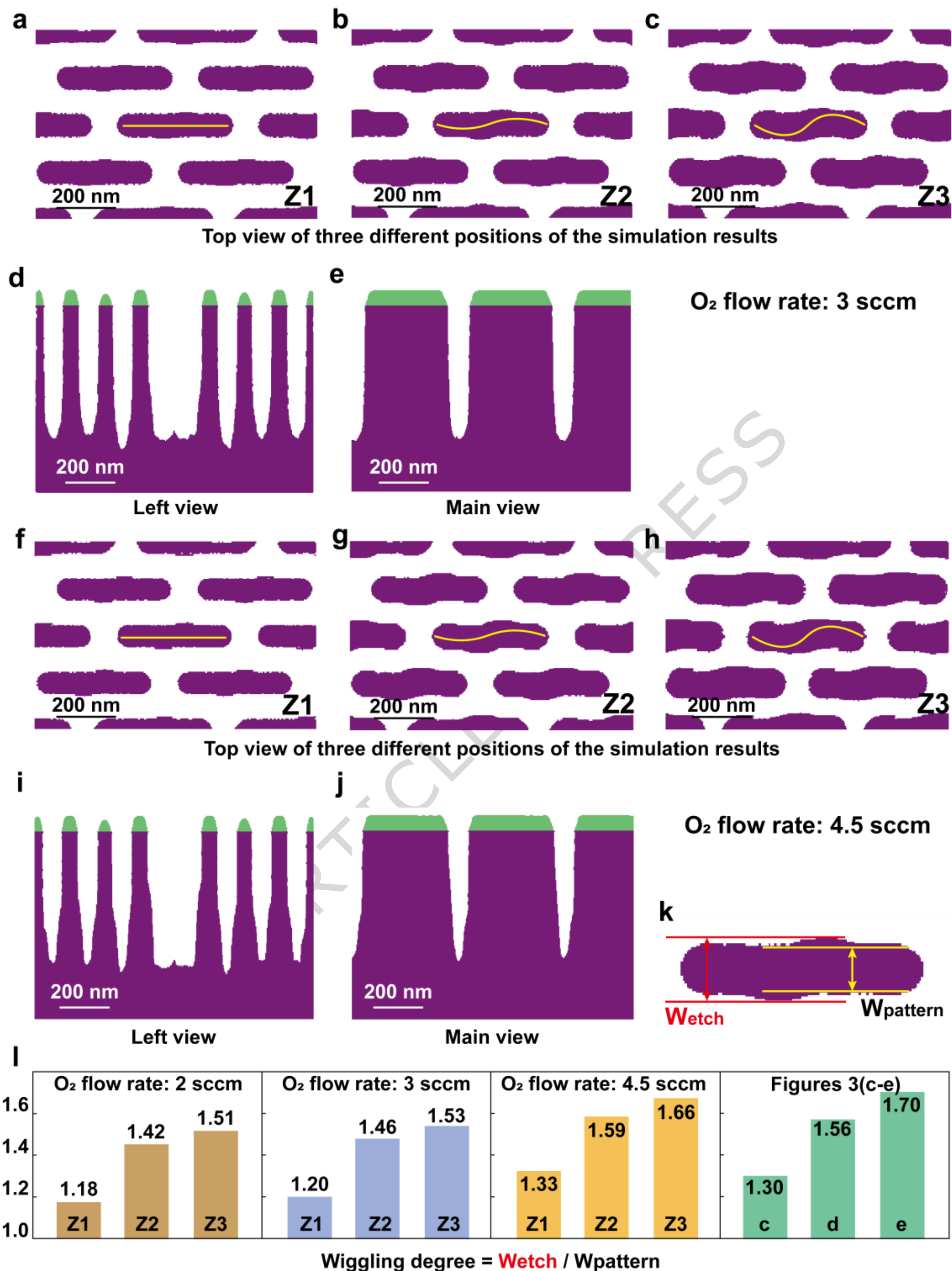

Figure 6. Cross-sectional analysis and wiggling degree quantification of 3D simulation results under different oxygen flow rates. a-c) Cross-sections obtained by slicing planes parallel to the wafer surface in the 3D simulation result with an oxygen flow rate of 3 sccm, a corresponds to the shallowest position (Z1 = 100 nm), b corresponds to the shallowest position (Z2 = 300 nm), c

corresponds to the deepest (Z3 = 500 nm). d) Cross-section obtained by cutting parallel to the SEM shooting surface. e) Cross-section obtained by cutting perpendicular to SEM shooting surface. f-h) Cross-sections obtained by cutting parallel to the wafer surface in the 3D simulation result at an oxygen flow rate of 4.5 sccm, where f corresponds to the shallowest position (Z1 = 100 nm), g corresponds to the shallowest position (Z2 = 300 nm), h corresponds to the deepest (Z3 = 500 nm). i) Cross-section obtained by slicing planes parallel to the SEM shooting surface in the 3D simulation results. j) Cross-section obtained by slicing 2D planes perpendicular to SEM shooting surface. k) Wiggling degree measurement and calculation method. l) Wiggling degree calculation of the simulation results and the 3D reconstruction results at different depths under different oxygen flow rates. The yellow lines in panels (a, b, c, f, g, h) trace the amplitude of wiggling. Throughout all panels (a-k), the purple and green objects represent the silicon (Si) and silicon dioxide (SiO_2) materials, respectively.

ARTICLE IN PRESS

Conclusions

In this study, to investigate the wiggling AA effect observed during plasma etching in advanced DRAM architectures, we fabricated the active area transistors of DRAM structures on silicon wafers using EBL and ICP dry etching. The etching results were characterized through SEM and 3D reconstruction based on FIB-SEM data. Meanwhile, we developed a 3D etching feature profile model that correlates process parameters with structural deformation, and systematically simulated the etching processes under three oxygen flow rates (2, 3, and 4.5 sccm). The mechanism of the wiggling AA effect is revealed by comparing the simulation results with experiments. The loading effect causes different amounts of by-product deposition in the sidewalls at different opening locations, which leads to wiggling AA. We further found that by reducing the oxygen flow rate, the wiggling degree is reduced. These findings provide both fundamental insights into plasma-surface interactions and a practical guideline for optimizing etching recipes in advanced DRAM manufacturing. Building upon this mechanistic understanding, future work should address the wafer-scale uniformity of the wiggling effect - a critical challenge for high-volume production influenced by pattern density variations and process gradients.

Methods

Fabrication flow setup and characterization method

Fabrication flow setup

ARTICLE IN PRESS

The silicon wafer used in the experiment was an 8-in p-type monocrystalline silicon (100) with an average resistivity of 0.5-100 Ω·m. First, an oxide layer (SiO_2) with a thickness of 80 nm was deposited on the bulk silicon surface using the plasma enhanced chemical vapor deposition tool (AMAT ENDURA). Then, an amorphous silicon (α-Si) film with a thickness of 50 nm was grown using a dielectric layer chemical enhanced vapor deposition tool (FPODUCER III). Next, the electron beam lithography (EBL) of the fin array pattern was performed using NanoBeam NB5 (NBL). Following that, the etch tool ALLIANCE Exelan HPT (Lam Research Corporation) was used to open the amorphous silicon and silicon dioxide hard mask with using a gas mixture of $CF_4/HBr/O_2$. Finally, the Si substrate anisotropic etching was performed with an HBr/O_2 gas mixture in an ICP reactor (Lam TCP 9400DFM). The reactor parameters in the Si etch step process are pressure: 50 mTorr / source power: 600W (13.56 MHz) / bias voltage: -200 V / flux: 100 sccm HBr, 2/3/4.5 sccm O_2 / chuck temperature: 300 K.

3D reconstruction flow

3D reconstruction of the results was performed using FIB tomography (Zeiss Crossbeam 550). Prior to milling, a dual-layer platinum (Pt) protective coating was deposited through sequential electron beam- and ion beam-induced deposition to preserve surface features that are vulnerable to ion beam damage. The automated milling process precisely controlled 3.5 nm as inter-slice spacing, which exceeded the current limit milling size. During the serial sectioning procedure, we were able to obtain the data set we need for 3D reconstruction. Finally, the data set was reconstructed using the Dragonfly software.

3D etching feature profile simulation model

The etching process simulations in this study were conducted using our in-house developed simulation model. This model incorporates the following core computational modules: simulation domain and particle incidence distribution settings, Monte Carlo trajectory tracking, particle reflection calculation, and surface chemical reactions.

Simulation domain and particles incident distribution settings

As illustrated in **Figure 4(c)**, in this study, we divide the three-dimensional etch structure into a $x \times y \times z$ grid for a window size of $length \times width \times height$ nm^3 with a fixed resolution using the voxel method. We adopted a numerical labeling system to represent the presence of different types of materials/states in each cell. There are four basic types of materials/states: 0-vacuum, 1-substrate/by-product, 2-hard mask, 3-particle. Consequently, along with the incidence of particles, more and more substrate or hard mask voxels will change into vacuum or by-product. Thus, this

ARTICLE IN PRESS

ARTICLE IN PRESS

model provides a real-time simulation of the etching profile. The incident site distribution of particles obeys a uniform distribution, which covers the entire plasma distribution area [29].

This model focuses on the transport of neutral species and surface reaction kinetics, which are identified as the primary factors governing the etching profile and wiggling morphology under our investigated conditions. A key simplification is the treatment of ion trajectories as predefined, without self-consistently solving for plasma sheath potentials or local electric fields. This approach is justified as it allows us to evaluate the dominant role of chemical transport and surface passivation, which is strongly suggested by the pronounced sensitivity of the etch profiles to the O_2 flow rate observed in our experiments. The model mainly considers two types of incident particles: isotropic incident particles (representing neutral species) and anisotropic incident particles (representing charged ions). The incidence angle distribution of isotropic incident particles follows the cosine distribution [30]. The incidence angle distribution of anisotropic incident particles obeys the Gaussian distribution where the mean μ represents the center incident angle, which is normal to the substrate, while the standard deviation σ represents the degree of the incident angle dispersion around the normal direction [31]. In this study, μ is set to 0 and σ is set to 0.035, corresponding to 99.7% of anisotropic incident particles within ±5.73°.

The fluxes of these species were estimated based on the fundamental process parameters that govern the plasma state: the inlet gas flow ratios ($HBr:O_2$), chamber pressure, and source power. The flux ratio between neutral Br and O atoms was scaled directly with the $HBr:O_2$ flow ratio, reflecting their origin from gas-phase dissociation. The absolute ion flux was calibrated against the plasma density, which is primarily governed by the source power under our operating pressure. This estimation framework was validated by ensuring the simulated etch depth matched the experimental trend. Consequently, the flux ratios employed in the simulations for the three oxygen flow conditions are Br : O : ions = 90 : (2, 3, or 4.5) : 10, where the oxygen flux varies with its set flow rate while the Br and ion fluxes are kept constant. The etch yield for silicon by ions is treated as angle-dependent but energy-independent for simplicity in this study.

Monte Carlo trajectory tracking

Once a particle is initiated from the plasma region with a fixed site and a fixed angle, it will move ballistically until it reaches the substrate surface and stop. Since the simulation domain is divided into a large number of voxels, the step sum method is used to track the particle trajectory. As shown in **Figure 4(d)**, each cycle will increase the length of a grid in the z direction (Δz = 1 unit height), calculate the offset (Δx and Δy) in the x and y direction through the particle incident angle, and judge the state of the upper and lower voxels at the new site. i) If the upper voxel is the

ARTICLE IN PRESS

substrate, the particle reacts with the substrate at the upper voxel, ii) if only the lower voxel cell is the substrate, the particle reacts with the lower voxel, iii) if both the upper and lower voxels are vacuum, the downward cycle continues to add steps until the reaction site is found.

Particle reflection calculation

During the Monte Carlo trajectory tracking, particles may be reflected after they reach the surface. Energetic ions can undergo specular or quasi-specular reflection (Conal distribution) depending on incidence angle and surface conditions, while neutrals generally have low energy and are more likely to scatter diffusely without significant reflection (Cosine distribution). Since the model discretizes the simulation domain, it is necessary to fit the surface before computing the incident angle of the particle on the surface. In our model, we select the surface voxels based on a 9×9×9 window size around the impact site as shown in **Figure 4(e)**. Then, we use least-square fitting to obtain a plane representative of the surface normal for these surface voxels [32]. The fitting process is shown in Supplementary Note 1. Particles that hit the surface with a large incidence angle will have larger reflection probability, and their contribution to the surface reaction will be reduced [33]. Based on this observation, the reflection probability as follows:

$$P_R = \begin{cases} 0 & , \quad \theta < \theta_{\mathrm{th}} \\ \frac{(\theta - \theta_{\mathrm{th}})}{\frac{\Pi}{2} - \theta_{\mathrm{th}}} & , \quad \theta \geq \theta_{\mathrm{th}} \end{cases} \tag{1}$$

θ represents the incidence angle, θ_{th} represents the reflection angle threshold. Subsequently, we bring the P_R into the model, and the reflected particles will re-emit and hit another surface site. In this study, considering the computational complexity and error, model only considers one reflection [34].

Surface reactions

In this work, we study the etching of silicon substrate material, with silicon oxide as the hard mask, during etching in a bromine-based plasma (containing low concentrations of oxygen) with an ICP etcher as the reagent [35, 36]. We assume bromine neutral particles (Br), hydrogen particles (H) and oxygen (O and O_2) are isotropic incident particles, and bromine ions (Br^+) are anisotropic incident particles. When the incident particles strike the substrate surface, several surface reactions will take place in the actual process, resulting in the formation of intermediate products or by-products into the reactor. In our model, to simplify the reactions, we assume reasonable probabilities for reactions and bring them into our model [37-39]. These reactions and probabilities are determined from the literature and listed in **Table 2**.

ARTICLE IN PRESS

Tabel 2. Surface reactions and probabilities.

Reaction	Probability	Reference
$Br_{(g)} + Si_{(s)} \rightarrow SiBr_{(s)}$	0.99	37
$Br_{(g)} + SiBr_{(s)} \rightarrow SiBr_{2(s)}$	0.95	37
$Br_{(g)} + SiBr_{2(s)} \rightarrow SiBr_{3(s)}$	0.9	37
$Br_{(g)} + SiBr_{3(s)} \rightarrow SiBr_{4(g)}$	0.01	37
$Br_{(g)} + SiH_xBr_{y(s)} \rightarrow SiH_xBr_{y+1(s)}$ $(3 \geq x + y \geq 1; x \geq 1)$	0.5	37
$H_{(g)} + SiH_xBr_{y(s)} \rightarrow SiH_{x+1}Br_{y(s)}$ $(3 \geq x + y \geq 0)$	0.5	37
$Br_{(g)} + SiH_xBr_{y-1(s)} \rightarrow SiH_xBr_{y(g)}$ $(x + y = 4; x \geq 1, y \geq 1)$	0.001	37
$H_{(g)} + SiH_{x-1}Br_{y(s)} \rightarrow SiH_xBr_{y(g)}$ $(x + y = 4; x \geq 1)$	0.001	37
$Br^+ + SiBr_{x(s)} \rightarrow SiBr_{x(g)} + Br^*$ $(4 \geq x \geq 1)$ *	$\frac{x}{4} \times 0.8$	37
$Br^+ + SiH_xBr_{y(s)} \rightarrow SiH_xBr_{y(g)} + Br^*$ $(4 \geq x + y \geq 1; x \geq 1)$ *	$\frac{x+y}{4} \times 0.8$	37
$O_{(g)} + Si_{(s)} \rightarrow SiO_{(s)}$	0.99	38
$O_{(g)} + SiO_{(s)} \rightarrow SiO_{2(s)}$	0.99	38
$O_{2(g)} + Si_{(s)} \rightarrow SiO_{2(s)}$	0.01	38
$O_{2(g)} + SiO_{(s)} \rightarrow SiO_{2(s)} + O_{(g)}$	0.01	38
$Si_{(s)} + 2H_2O_{(g)} \rightarrow SiO_{2(s)} + 2H_{2(g)}$	0.2	39
$SiO_{2(s)} + 4H_{(g)} \rightarrow Si_{(s)} + 2H_2O_{(g)}$	0.1	39

*The motion trajectory and subsequent reaction of Br^* are not considered in this study.

ARTICLE IN PRESS

Data Availability

ARTICLE IN PRESS

All data needed to evaluate the conclusions are present in the paper. Additional data and raw data are available upon request from the corresponding author.

Code Availability

All relevant code used to generate the results presented in this study is available from the corresponding author upon reasonable request.

References

[1] Belmonte, A., et al. "Capacitor-less, long-retention (> 400s) DRAM cell paving the way towards low-power and high-density monolithic 3D DRAM." *2020 IEEE International Electron Devices Meeting (IEDM)*. IEEE, 2020.

[2] Wang, Yin, et al. "An in-memory computing architecture based on two-dimensional semiconductors for multiply-accumulate operations." *Nature communications* 12.1 (2021): 3347.

[3] Hu, Qianlan, et al. "Optimized IGZO FETs for capacitorless DRAM with retention of 10 ks at RT and 7 ks at 85° C at zero V hold with sub-10 ns speed and 3-bit operation." *2022 International Electron Devices Meeting (IEDM)*. IEEE, 2022.

[4] Sankpal, Amol S., and D. J. Pete. "Study and Analysis of Leakage current and leakage power in 1T1C DRAM at Nano Scale Technology." *2020 4th International Conference on Electronics, Communication and Aerospace Technology (ICECA)*. IEEE, 2020.

[5] Kimura, S., et al. "A diagonal active-area stacked capacitor DRAM cell with storage capacitor on bit line." *IEEE Transactions on Electron Devices* 37.3 (1990): 737-743.

[6] Spessot, Alessio, and Hyungrock Oh. "1T-1C dynamic random access memory status, challenges, and prospects." *IEEE Transactions on Electron Devices* 67.4 (2020): 1382-1393.

[7] Wang, QingPeng, et al. "A Study of Wiggling AA modeling and Its Impact on the Device Performance in Advanced DRAM." *2020 International Conference on Simulation of Semiconductor Processes and Devices (SISPAD)*. IEEE, 2020.

[8] LPDDR4 SDRAM 1x nm tear down report from TechInsights.

[9] GANESH, DE. "A Complete study and review of Characterization Techniques of Nano materials." *Global Journal of Research in Engineering & Computer Sciences* 2.2 (2022).

[10] Ma, Zhiliang, and Shilong Liu. "A review of 3D reconstruction techniques in civil engineering and their applications." *Advanced Engineering Informatics* 37 (2018): 163-174.

[11] Zhao, Zhi, and Xiao-Ping Zhou. "An integrated method for 3D reconstruction model of porous geomaterials through 2D CT images." *Computers & Geosciences* 123 (2019): 83-94.

ARTICLE IN PRESS

ARTICLE IN PRESS

[12] Chitsaz, Nasim, Romeo Marian, and Javaan Chahl. "Experimental method for 3D reconstruction of Odonata wings (methodology and dataset)." *PLoS One* 15.4 (2020): e0232193.

[13] Nan, Nan, and Jingxin Wang. "FIB-SEM three-dimensional tomography for characterization of carbon-based materials." *Advances in Materials Science and Engineering* 2019.1 (2019): 8680715.

[14] Dreier, T., D. Nilsson, and J. Hållstedt. "Fast and high-resolution X-ray nano tomography for failure analysis in advanced packaging." Microelectronics Reliability 168 (2025): 115694.

[15] Yuchen, Fan, and Liu Keyu. "Large-volume FIB-SEM 3D reconstruction: An effective method for characterizing pore space of lacustrine shales." *Frontiers in Earth Science* 10 (2023): 1046927.

[16] Raffa, V., Castrataro, P., Menciassi, A., Dario, P. (2006). Focused Ion Beam as a Scanning Probe: Methods and Applications. In: Bhushan, B., Fuchs, H. (eds) Applied Scanning Probe Methods II. Nano Science and Technology. Springer, Berlin, Heidelberg. https://doi.org/10.1007/3-540-27453-7_11

[17] Hoekstra, Robert J., and Mark J. Kushner. "Comparison of two-dimensional and three-dimensional models for profile simulation of poly-Si etching of finite length trenches." *Journal of Vacuum Science & Technology A: Vacuum, Surfaces, and Films* 16.6 (1998): 3274-3280.

[18] Zhang, Yiting, et al. "Investigation of feature orientation and consequences of ion tilting during plasma etching with a three-dimensional feature profile simulator." *Journal of Vacuum Science & Technology A* 35.2 (2017).

[19] Yook, Yeong Geun, et al. "Fast and realistic 3D feature profile simulation platform for plasma etching process." *Journal of Physics D: Applied Physics* 55.25 (2022): 255202.

[20] Wu, Cheng-En, et al. "Photoresist 3D profile related etch process simulation and its application to full chip etch compact modeling." *Optical Microlithography XXVIII*. Vol. 9426. SPIE, 2015.

[21] Moroz, Paul, and Daniel J. Moroz. "Feature profile 2D and 3D simulation with etching, deposition, and implantation processes." *ECS Transactions* 50.46 (2013): 61.

[22] Ren, Qianhui, et al. "3D X-ray microscope acts as an accurate and effective equipment of pathological diagnosis in craniofacial imaging." *Scientific Reports* 14.1 (2024): 23275.

[23] Xu, C. Shan, Kenneth J. Hayworth, and Harald F. Hess. "Enhanced FIB-SEM systems for large-volume 3D imaging." U.S. Patent No. 10,600,615. 24 Mar. 2020.

[24] Mura, Francesco, et al. "Advances in focused ion beam tomography for three-dimensional characterization in materials science." *Materials* 16.17 (2023): 5808.

[25] Miyake, Masatoshi, et al. "Effects of mask and necking deformation on bowing and twisting

ARTICLE IN PRESS

ARTICLE IN PRESS

in high-aspect-ratio contact hole etching." Japanese Journal of Applied Physics 48.8S1 (2009): 08HE01.

[26] Negishi, Nobuyuki, et al. "Bottom profile degradation mechanism in high aspect ratio feature etching based on pattern transfer observation." Journal of Vacuum Science & Technology B 35.5 (2017).

[27] Fried, D., et al. "Predictive modeling of pattern-dependent etch effects in large-area fully-integrated 3D virtual fabrication." *2014 International Conference on Simulation of Semiconductor Processes and Devices (SISPAD)*. IEEE, 2014.

[28] Haass, Moritz, et al. "Silicon etching in a pulsed HBr/O2 plasma. I. Ion flux and energy analysis." Journal of Vacuum Science & Technology B 33.3 (2015).

[29] Iza, Felipe, et al. "Microplasmas: Sources, particle kinetics, and biomedical applications." *Plasma Processes and Polymers* 5.4 (2008): 322-344.

[30] Costin, C. "Particle distribution functions at plasma–surface interface." *AIP Advances* 10.11 (2020).

[31] Zhang, Peng, Lidan Zhang, and Lan Xu. "Study on the influence of electron angular distribution on mask pattern damage in plasma etching." *Plasma Processes and Polymers* 17.7 (2020): 2000014.

[32] Xue, Lihong, and Dongping Li. "Research on piecewise linear fitting method based on least square method in 3D space points." *The Open Automation and Control Systems Journal* 7.1 (2015).

[33] Hatsuse, Takumi, et al. "Origin of plasma-induced surface roughening and ripple formation during plasma etching: The crucial role of ion reflection." *Journal of Applied Physics* 124.14 (2018).

[34] Laroussi, Mounir, and J. Reece Roth. "Numerical calculation of the reflection, absorption, and transmission of microwaves by a nonuniform plasma slab." *IEEE Transactions on Plasma Science* 21.4 (1993): 366-372.

[35] Tinck, S., W. Boullart, and A. Bogaerts. "Modeling Cl2/O2/Ar inductively coupled plasmas used for silicon etching: effects of SiO2 chamber wall coating." *Plasma Sources Science and Technology* 20.4 (2011): 045012.

[36] Mori, Masahito, et al. "Formation mechanisms of etched feature profiles during Si etching in Cl2/O2 plasmas." *Journal of Vacuum Science & Technology A* 37.5 (2019).

[37] Mori, Masahito, et al. "Model analysis of the feature profile evolution during Si etching in HBr-containing plasmas." *Journal of Vacuum Science & Technology A* 39.4 (2021).

[38] Tinck, S., W. Boullart, and A. Bogaerts. "Modeling Cl2/O2/Ar inductively coupled plasmas used for silicon etching: effects of SiO2 chamber wall coating." *Plasma Sources Science and Technology* 20.4 (2011): 045012.

ARTICLE IN PRESS

ARTICLE IN PRESS

[39] Wen-Shiang Liao, Si-Chen Lee; Water-induced room-temperature oxidation of Si–H and –Si–Si– bonds in silicon oxide. *J. Appl. Phys.* 15 July 1996; 80 (2): 1171–1176.

Acknowledgements

Supported by the National Key R&D Program of China (No. 2023YFB4402600), the National Natural Science Foundation of China (No. 62474194), the International Partnership Program of the Chinese Academy of Sciences (No.102GJHZ2024059GC and 102GJHZ2024029FN). Supported by the Austrian Federal Ministry of Labour and Economy, the National Foundation for Research, Technology and Development, and the Christian Doppler Research Association, Austria.

Author contributions

Ziyi Hu: Conceptualization; Formal analysis; Investigation; Methodology; Project administration; Software; Validation; Visualization; Writing - original draft; Writing - review & editing. **Jing Wen**: Investigation; Methodology; Writing - original draft. **Chaoran Yang**: Investigation; Methodology. **Hua Shao**: Investigation; Validation. **Yuxuan Zhai**: Investigation; Validation. **Rui Ge**: Investigation; Validation. **Xiaobin He**: Investigation. **Zongzheng Men**: Investigation; Methodology. **Yi Yang**: Investigation; Methodology. **Dianming Sun**: Investigation; Methodology. **Zhongming Liu**: Investigation; Methodology. **Dashan Shang**: Writing - original draft; Writing - review & editing. **Zhiqiang Li**: Validation. **Junjie Li**: Conceptualization; Validation; Writing - original draft. **Lado Filipovic**: Funding acquisition; Validation; Writing - review & editing. **Rui Chen**: Funding acquisition; Investigation; Project administration; Resources; Supervision; Writing - original draft; Writing - review & editing. **Ling Li**: Funding acquisition; Project administration.

Competing interests

The authors declare no competing interests

ARTICLE IN PRESS

ARTICLE IN PRESS

Editor's Summary:

Ziyi Hu and colleagues report a combined 3D reconstruction and simulation method to reveal the cause of the wiggling effect in advanced Dynamic Random Access Memory. This method provides a tool for etching process optimization to improve reliability.

Peer review information:

Communications Engineering thanks Du Zhang and the other, anonymous, reviewer(s) for their contribution to the peer review of this work. Primary Handling Editors: [Philip Coatsworth]. A peer review file is available.

ARTICLE IN PRESS